

Models of Neutrino Masses: Anarchy versus Hierarchy

Guido Altarelli ¹

Theory Division, CERN,
CH-1211 Genève 23, Switzerland

Ferruccio Feruglio ²,

Dipartimento di Fisica 'G. Galilei', Università di Padova and
INFN, Sezione di Padova, Via Marzolo 8, I-35131 Padua, Italy

Isabella Masina ³,

Service de Physique Théorique, CEA-Saclay
F-91191 Gif-sur-Yvette, France

Abstract

We present a quantitative study of the ability of models with different levels of hierarchy to reproduce the solar neutrino solutions, in particular the LA solution. As a flexible testing ground we consider models based on $SU(5) \times U(1)_F$. In this context, we have made statistical simulations of models with different patterns from anarchy to various types of hierarchy: normal hierarchical models with and without automatic suppression of the 23 (sub)determinant and inverse hierarchy models. We find that, not only for the LOW or VO solutions, but even in the LA case, the hierarchical models have a significantly better success rate than those based on anarchy. The normal hierarchy and the inverse hierarchy models have comparable performances in models with see-saw dominance, while the inverse hierarchy models are particularly good in the no see-saw versions. As a possible distinction between these categories of models, the inverse hierarchy models favour a maximal solar mixing angle and their rate of success drops dramatically as the mixing angle decreases, while normal hierarchy models are far more stable in this respect.

¹e-mail address: guido.altarelli@cern.ch

²e-mail address: feruglio@pd.infn.it

³e-mail address: masina@sptt.saclay.cea.fr

1 Introduction

At present there are many possible models of ν masses and mixing [1]. This variety is mostly due to the considerable experimental ambiguities that remain. In particular different solutions for solar neutrino oscillations are still possible. Although the Large Angle (LA) solution emerges as the most likely from present data, the other solutions LOW and Vacuum Oscillations (VO) are still not excluded (the small angle solution is very disfavoured by now and we will disregard it in most of the following discussion). Indeed no solution is actually leading to an imposingly good fit and, for example, the discrimination between LA and LOW is only based on a few hints which are far from compelling [2]. Hopefully in a few months, when the first results from the KamLAND experiment [3] will be known, one will have decisive evidence on this matter. Here we tentatively disregard the possibility of a third neutrino oscillation frequency as indicated by the LSND experiment [4] but not confirmed by KARMEN [5] and to be finally checked by the MiniBOONE experiment [6] now about to start.

For model building there is an important quantitative difference between the LA solution on the one side and the LOW or VO solutions on the other side. While for all these solutions the relevant mixing angle θ_{12} is large, the value of the squared mass difference $\Delta m_{12}^2 = m_2^2 - m_1^2$ (with, by definition, $m_2^2 \geq m_1^2$) is very different for LA, LOW and VO: $\sim 10^{-4} eV^2$, $\sim 10^{-7} eV^2$ and $\sim 10^{-10} eV^2$, respectively. Thus the gap with respect to the atmospheric neutrino oscillation frequency $\Delta m_{23}^2 = m_3^2 - m_2^2$, which is given by $|\Delta m_{23}^2| \sim 3 \cdot 10^{-3} eV^2$, is moderate for LA and very pronounced for the other two solutions.

For the LOW and VO solutions the large frequency difference with respect to that of atmospheric neutrinos points to a hierarchical spectrum for the three light neutrinos. Possible hierarchical patterns are the normal hierarchy case $m_3 \gg m_2 \gtrsim m_1$ or the inverted hierarchy alternative $m_2 \gtrsim m_1 \gg m_3$ (in this case Δm_{23}^2 is negative in our definition). Then a main problem is to explain the presence of large mixing angles between largely splitted mass states (in particular the atmospheric neutrino oscillation mixing angle θ_{23} is experimentally close to maximal). In hierarchical models the consistency of these usually opposed constraints is obtained by mechanisms that guarantee a vanishing or a strongly suppressed 23 sub-determinant. In the see-saw mechanism for neutrino masses this suppression can be naturally obtained, for example, in the so-called lopsided models [7] and/or by the dominance [8] of one eigenvalue in M^{-1} , M being the right-handed (RH) Majorana matrix. Models of this type have been studied and provide, as also quantitatively confirmed by our present analysis, an essentially unique framework for a successful description of both atmospheric and solar neutrino oscillations when the LOW or the VO solutions are adopted.

In the case of the LA solution the ratio of the solar and atmospheric Δm^2 ranges is typically given by

$$r = \Delta m_{12}^2 / |\Delta m_{23}^2| \sim 1/20 - 1/100. \quad (1)$$

For LA one can reproduce the data either in a nearly degenerate or in a hierarchical model. In a degenerate model, due to laboratory and cosmological bounds, the common value of $m_i^2 \sim m^2$ cannot exceed a few eV^2 . But the actual value is probably well below this level because of the constraint imposed by neutrinoless double beta decay ($0\nu\beta\beta$) [9] that would otherwise require a strong cancellation, only possible for nearly maximal solar oscillation mixing [10]. This fact, together with the general difficulty, in the absence of a specific mechanism, of obtaining too small values of $\Delta m_{12}^2/m^2$, suggests that a moderate degeneracy is more likely. Typically we could have all $m_i^2 \sim (\text{few } 10^{-3} - 10^{-2}) eV^2$ with one comparatively not-so-small splitting $\Delta m_{12}^2 \sim 10^{-4} eV^2$. Or, as a different example, we can have a (normal) hierarchical model with $m_3^2 \sim 3 \cdot 10^{-3} eV^2$, $m_2^2 \lesssim 10^{-4} eV^2$ and $m_1^2 \sim 0$ or an (inverse) hierarchical model with $m_{1,2}^2 \sim 3 \cdot 10^{-3} eV^2$, and $m_3^2 \sim 0$. Actually a sufficient hierarchy (a factor of 5 in mass) can arise from no significant underlying structure at all. In particular, the see-saw mechanism, being quadratic in the Dirac neutrino masses, tends to enhance small fluctuations in the Dirac eigenvalue ratios. This is the point of view of anarchical models [11], where no structure is assumed to exist in the neutrino mass matrix and the smallness of r is interpreted as a fluctuation. But one additional feature of the data plays an important role in this context and presents a clear difficulty for anarchical models. This is the experimental result that the third mixing angle θ_{13} is small, $|U_{e3}| = |\sin \theta_{13}| \lesssim 0.2$ [12]. So, for neutrinos two mixing angles are large and one is small. Instead in anarchical models all angles should a priori be comparable and not particularly small. Therefore this is a difficulty for anarchy and, for the survival of these models, it is necessary that θ_{13} is found very close to the present upper bound. Instead in hierarchical models the smallness of θ_{13} can be obtained as a reflection of the underlying structure in that some small parameter is present from the beginning in these models.

In this note we make a quantitative study of the ability of different models to reproduce the solar neutrino solutions. As a flexible testing ground we consider models based on $SU(5) \times U(1)_F$. The $SU(5)$ generators act “vertically” inside one generation, while the $U(1)_F$ charges are different “horizontally” from one generation to the other. If, for a given interaction vertex, the $U(1)_F$ charges do not add to zero, the vertex is forbidden in the symmetric limit. But the symmetry is spontaneously broken by the VEV v_f of a number of “flavon” fields with non vanishing charge. Then a forbidden coupling is rescued but is suppressed by powers of the small parameters $\lambda_f = v_f/\Lambda$ with the exponent larger for larger charge mismatch [13]. We expect $v_f \gtrsim M_{GUT}$ and, for the cut-off Λ of the theory, $\Lambda \lesssim M_{Pl}$. In these models [14, 15]

the known generations of quarks and leptons are contained in triplets Ψ_i^{10} and $\Psi_i^{\bar{5}}$, ($i = 1, 2, 3$) corresponding to the 3 generations, transforming as 10 and $\bar{5}$ of SU(5), respectively. Three more SU(5) singlets Ψ_i^1 describe the RH neutrinos. In SUSY models we have two Higgs multiplets, which transform as 5 and $\bar{5}$ in the minimal model. All mass matrix elements are of the form of a power of a suppression factor times a number of order unity, so that only their order of suppression is defined. We restrict for simplicity to integral charges: this is practically a forced choice for the LA case where the hierarchy parameter must be relatively large (so that $\sqrt{\lambda} \sim 0(1)$), while for the LOW and VO cases, where the hierarchy parameter is small, it is only motivated by the fact that enough flexibility is obtained for the present indicative purposes. There are many variants of these models [1]: fermion charges can all be non negative with only negatively charged flavons, or there can be fermion charges of different signs with either flavons of both charges or only flavons of one charge. The Higgs charges can be equal, in particular both vanishing or can be different. We will make use of this flexibility in order to study the relative merits of anarchy versus various degrees and different patterns of hierarchy.

In this context we have studied in detail different classes of models: normal hierarchical models with and without automatic suppression of the 23 (sub)determinant, inverse hierarchy models and anarchical models. The normal hierarchical models without automatic suppression of the 23 determinant are clearly intermediate: in a sense in those cases anarchy is limited to the 23 sector. We denote them as partially hierarchical or semi-anarchical in the following. We also compare, when applicable, models with light neutrino masses dominated by the see-saw mechanism or by non renormalizable dim-5 operators. We construct our models by assigning suitable sets of charges for Ψ_i^{10} , $\Psi_i^{\bar{5}}$ and Ψ_i^1 . In all input mass matrices the coefficients multiplying the power of the hierarchy parameter are generated at random as real and complex numbers in a given range of values [11, 16]. We compare the case of real or complex parameters and we also discuss the delicate questions of the probability distribution for the coefficients and the stability of the results. We assign a merit factor to each model given by the percentage of success over a large sample of trials. For each model the value of the hierarchy parameter is adjusted by a coarse fitting procedure to get the best rate of success.

Our results can be summarized as follows. As expected, for the LOW and VO cases only hierarchical model provide a viable approach: in comparison the rate of success of anarchical and seminarchical models is negligible. But also for the LA solution we still find that hierarchical models are sizeably better in general. The most efficient ones are inverse hierarchy models with no see-saw dominance, which are more than 10 times better with respect to anarchy with see-saw (anarchy prefers the see-saw case by about a factor of 2). Among the see-saw dominance versions the most performant models remain the hierarchical ones (by a factor of

about 4 with respect to anarchy with see-saw) with not much difference between inverse or normal hierarchy. Semi-Anarchical models are down by a factor of about 2 with respect to hierarchical models among the see-saw versions (but this value is less stable with respect to changes of the extraction procedure and, for example, it tends to be washed out going from complex to real coefficients). In all models the $\tan^2 \theta_{23}$ distribution is in agreement with large mixing but it is not sharply peaked around 1 as for maximal mixing. Near maximal mixing is instead a prediction for solar neutrinos in inverse hierarchical models, so that their advantage with respect to other models would be rapidly destroyed if the data will eventually move in the direction away from maximality.

2 Framework

We consider a class of models with an abelian flavour symmetry compatible with SU(5) grand unification. Here we will not address the well-known problems of grand unified theories, such as the doublet-triplet splitting, the proton lifetime, the gauge coupling unification beyond leading order and the wrong mass relations for charged fermions of the first two generations. We adopt the $SU(5) \times U(1)_F$ framework simply as a convenient testing ground for different neutrino mass scenarios. In all the models that we study the large atmospheric mixing angle is described by assigning equal flavour charge to muon and tau neutrinos and their weak SU(2) partners (all belonging to the $\bar{5} \equiv (l, d^c)$ representation of SU(5)). Instead, the solar neutrino oscillations can be obtained with different, inequivalent charge assignments and both the LOW¹ and the LA solution can be reproduced.

A first class of models is characterized by all matter fields having flavour charges of one sign, for example all non negative. An important property of models in this class is that the light neutrino mass matrix $L^T m_\nu L$ is independent from the charges of both the $10 \equiv (q, u^c, e^c)$ and $1 \equiv \nu^c$ representations, even in the see-saw case when $m_\nu = m_D^T M_R^{-1} m_D$. For m_ν entries the powers of the symmetry breaking parameter λ are dictated by the charges F of the $\bar{5}$. Since in this case what really matters are charge differences, rather than absolute values, the equal charges for the second and third generations can be put to zero, without losing generality:

$$F(\bar{5}) = (b, 0, 0) \quad b \geq 0 \quad . \quad (2)$$

If b also vanishes, then the light neutrino mass matrix will be structure-less and we will call anarchical (A) this sub-class of models. In a large sample of anarchical

¹The LOW and VO solutions can be fitted almost equally well by suitable models. Thus here we will focus mainly on the LOW case.

models, generated with random coefficients, the resulting neutrino mass spectrum can exhibit either normal or inverse hierarchy. Anarchical models clearly prefer the LA solution with a moderate separation between atmospheric and solar frequencies. They tend to favour large, not necessarily maximal, mixing angles, including U_{e3} , which represents a problem. Therefore, in anarchical models, U_{e3} is expected to be close to the present experimental bound.

If b is positive, then the light neutrino mass matrix will be structure-less only in the (2,3) sub-sector and we will call semi-anarchical (SA) the corresponding models. In this case, the neutrino mass spectrum has normal hierarchy. However, unless the (2,3) sub-determinant is accidentally suppressed, atmospheric and solar oscillation frequencies are expected to be of the same order and, in addition, the preferred solar mixing angle is small. Nevertheless, such a suppression can occur in a fraction of semi-anarchical models generated with random, order one coefficients. The real advantage over the fully anarchical scheme is represented by the suppression in U_{e3} .

In a second class of models matter fields have both positive and negative flavour charges. In these models, the light neutrino mass matrix will in general depend also on the charges of 10 and 1. A first sub-case arises when only the RH neutrino fields have charges of both signs. It has been shown that it is possible to exploit this feature to reproduce a neutrino mass spectrum with normal hierarchy and a natural gap between atmospheric and solar frequencies. Via the see-saw mechanism the (2,3) sub-determinant vanishes in the flavour symmetric limit. At the same time a large solar mixing angle can be obtained. Clearly this is particularly relevant for the LOW (or VO) solution. It is less clear to which extent the condition of vanishing determinant is needed for the LA solution and one of the purposes of the present paper is precisely to compare these models, which we will call hierarchical (H) with the anarchical and semi-anarchical models, that do not reproduce such a condition.

Finally, we can have fields with charges of both signs in both the 1 and the $\bar{5}$. In this context it is possible to reproduce an inverse hierarchical spectrum, with a large (actually, almost maximal) solar mixing angle and a large gap between atmospheric and solar frequencies [17]. Also this sub-class of models, which we call inversely hierarchical (IH), are appropriate to describe both LOW and LA solutions.

The hierarchical and the inversely hierarchical models may come into several varieties depending on the number and the charge of the flavour symmetry breaking (FSB) parameters. Here we will consider both the case (I) of a single, negatively charged flavon, with symmetry breaking parameter λ or that of two (II) oppositely charged flavons with symmetry breaking parameters λ and λ' . In case I, it is impossible to compensate negative F charges in the Yukawa couplings and the corresponding entries in the neutrino mass matrices vanish. Eventually these zeroes are filled by small contributions, arising, for instance, from the diagonalization of the charged lepton sector or from the transformations needed to make the kinetic terms canon-

Table 1: Models and their flavour charges.

Model	Ψ_{10}	$\Psi_{\bar{5}}$	Ψ_1	(H_u, H_d)
Anarchical (A)	(3,2,0)	(0,0,0)	(0,0,0)	(0,0)
Semi-Anarchical (SA)	(2,1,0)	(1,0,0)	(2,1,0)	(0,0)
Hierarchical (H)	(3,2,0)	(2,0,0)	(1,-1,0)	(0,0)
Inversely Hierarchical (LA)	(3,2,0)	(1,-1,-1)	(-1,+1,0)	(0,+1)
Inversely Hierarchical (LOW)	(2,1,0)	(2,-2,-2)	(-2,+2,0)	(0,+2)

ical. In our analysis we will always include effects coming from the charged lepton sector, whereas we will neglect those coming from non-canonical kinetic terms.

Another important ingredient in our analysis is represented by the see-saw mechanism [18]. Hierarchical models and semi-anarchical models have similar charges in the $(10, \bar{5})$ sectors and, in the absence of the see-saw mechanism, they would give rise to similar results. Even when the results are expected to be independent from the charges of the RH neutrinos, as it is the case for the anarchical and semi-anarchical models, the see-saw mechanism can induce some sizeable effect in a statistical analysis. For this reason, for each type of model, but the hierarchical ones (the mechanism for the 23 sub-determinant suppression is in fact based on the see-saw mechanism), we will separately study the case where RH neutrinos are present and the case where they are absent. When RH neutrinos are present, there are two independent contributions to the light neutrino mass matrix. One of them comes via the see-saw mechanism from the exchange of the heavy RH modes. The other one is provided by L-violating dimension five operators arising from physics beyond the cut-off. These contributions have the same transformation properties under the flavour group and, in general, add coherently. In our analysis we will analyze the case where the see-

saw contribution is the dominant one (SS). The absence of RH neutrinos describes the opposite case, when the mass matrix is saturated by the non-renormalizable contribution (NOSS).

For each type of model we have selected what we consider to be a typical representative ² and we have collected in table 1 the corresponding charges. In the next section we will compare the performances of the following models: A_{SS} , A_{NOSS} , SA_{SS} , SA_{NOSS} , $H_{(SS,I)}$, $H_{(SS,II)}$, $IH_{(SS,I)}$, $IH_{(SS,II)}$, $IH_{(NOSS,I)}$ and $IH_{(NOSS,II)}$.

Table 2: Order of magnitude predictions for oscillation parameters, from neutrino mass matrices in eq. (3) and (4) [1]; d_{23} denotes the sub-determinant in the 23 sector and we show the effect of its accidental suppression for the semi-anarchical model. In the estimates we have chosen $\lambda = \lambda'$. Inverse hierarchy predicts an almost maximal θ_{12} .

Model	parameters	d_{23}	$\Delta m_{12}^2/ \Delta m_{23}^2 $	U_{e3}	$\tan^2 \theta_{12}$	$\tan^2 \theta_{23}$
A	$\epsilon = 1$	O(1)	O(1)	O(1)	O(1)	O(1)
SA	$\epsilon = \lambda$	O(1)	$O(d_{23}^2)$	O(λ)	$O(\lambda^2/d_{23}^2)$	O(1)
H_{II}	$\epsilon = \lambda^2$	$O(\lambda^2)$	$O(\lambda^4)$	$O(\lambda^2)$	O(1)	O(1)
H_I	$\epsilon = \lambda^2$	0	$O(\lambda^6)$	$O(\lambda^2)$	O(1)	O(1)
IH (LA)	$\epsilon = \eta = \lambda$	$O(\lambda^4)$	$O(\lambda^2)$	$O(\lambda^2)$	$1+O(\lambda^2)$	O(1)
IH (LOW)	$\epsilon = \eta = \lambda^2$	$O(\lambda^8)$	$O(\lambda^4)$	$O(\lambda^4)$	$1+O(\lambda^4)$	O(1)

²We made no real optimization effort to pick up the ‘most’ representative, but rather a model with a high success rate in its class.

Anarchical, semi-anarchical and hierarchical models give rise to a mass matrix for light neutrinos of the type

$$m_\nu = \begin{pmatrix} \epsilon^2 & \epsilon & \epsilon \\ \epsilon & 1 & 1 \\ \epsilon & 1 & 1 \end{pmatrix} \quad (\text{A, SA, H}) \quad , \quad (3)$$

where all the entries are specified up to order one coefficients and the overall mass scale has been conventionally set to one. For anarchical models, $\epsilon = 1$. Then all the entries are uncorrelated numbers of order one and no particular pattern becomes manifest. For the semi-anarchical model of table 1, $\epsilon = \lambda$. There is a clear distinction between the first row and column and the 23 block of the mass matrix, which is structureless as in the anarchical models. In particular, barring accidental cancellations, the sub-determinant in the 23 sector is of order one. Finally, the hierarchical model defined by the choice of charges in table 1, has $\epsilon = \lambda^2$. At variance with the anarchical or semi-anarchical models, the determinant of the 23 sector is suppressed by the see-saw mechanism and is of order $\lambda\lambda'$.

The inversely hierarchical models are characterized by a neutrino mass matrix of the kind

$$m_\nu = \begin{pmatrix} \epsilon^2 & 1 & 1 \\ 1 & \eta^2 & \eta^2 \\ 1 & \eta^2 & \eta^2 \end{pmatrix} \quad (\text{IH}) \quad , \quad (4)$$

where $\epsilon = \lambda$ (λ^2) and $\eta = \lambda'$ (λ'^2) for the LA (LOW) solution. The ratio between the solar and atmospheric oscillation frequencies is not directly related to the sub-determinant of the block 23, in this case. The above mass matrices also receive an additional contribution from the diagonalization of the charged lepton sector, which, however, does not spoil the displayed structure. For completeness, we collect in table 2 the gross features of the models under consideration. Notice that the hierarchical models predict a ratio $\Delta m_{12}^2/|\Delta m_{23}^2|$ of order λ^4 or λ^6 . In these cases it is possible to fit both the LOW and the LA solutions with an expansion parameter $\lambda \approx \lambda'$ that, within a factor of two, matches the Cabibbo angle. On the contrary, the inversely hierarchical model that reproduces the LA solution favours $\Delta m_{12}^2/|\Delta m_{23}^2| \approx O(\lambda^2)$. If we adopt this model to fit also the LOW solution, the corresponding values of $\lambda \approx \lambda'$ do not provide a decent description of the remaining fermion masses. For this reason, when analyzing the LOW solution, we have considered a separate set of charges for the inverted hierarchy.

3 Method and results

Abelian flavour symmetries predict each entry of fermion mass matrices up to an unknown dimensionless coefficient. These coefficients, that are free-parameters of the theory, are expected to have absolute values of order one. Aside from generalized kinetic terms, which we do not consider, the relevant mass matrices are specified by $N = 24$ order one parameters: 9 from the charged lepton sector, 9 from Dirac neutrino mass matrix entries and 6 from Majorana RH neutrino mass matrices. When RH neutrinos are absent (that is, for the NOSS cases) the LH neutrino mass matrix contains 6 parameters and the relevant set reduces to $N = 15$ parameters. We have analyzed the case of real or complex coefficients $\mathcal{P} = (\mathcal{P}_1, \dots, \mathcal{P}_N)$, with absolute values generated as random numbers in an interval \mathcal{I} and random phases taken in $[0, 2\pi]$. To study the dependence of our results on \mathcal{I} , we have considered several possibilities: $[0.5, 2]$ (default), $[0.8, 1.2]$, $[0.95, 1.05]$ and $[0, 1]$. In the case of real coefficients, which is studied for comparison, we allow both signs for the coefficients. For each model, only a portion V_S of the volume $V = (2\pi\mathcal{I})^N$ of the parameter space gives rise to predictions in agreement with the experimental data within the existing uncertainties. We may interpret V_S/V as the success rate of the model in describing neutrino data. Clearly this portion shrinks to zero for infinitely good measurements. Therefore we are not interested in its absolute size, but rather in the relative sizes of V_S/V in different models.

We evaluate the success rate of each model by considering, through a random generation, a large number of ‘points’ \mathcal{P} and by checking whether the corresponding predictions do or do not fall in the experimentally allowed regions [16]. To this purpose we perform a test based on four observable quantities: $O_1 = r \equiv \Delta m_{12}^2/|\Delta m_{23}^2|$, $O_2 = \tan^2 \theta_{12}$, $O_3 = |U_{e3}| \equiv |\sin \theta_{13}|$ and $O_4 = \tan^2 \theta_{23}$. We take [19]:

$$\begin{aligned}
 &4 \cdot 10^{-6} < r < 4 \cdot 10^{-5} \\
 &|U_{e3}| < 0.2 \\
 &0.52 < \tan^2 \theta_{12} < 1.17 \\
 &0.33 < \tan^2 \theta_{23} < 3.3
 \end{aligned}
 \tag{LOW} \tag{5}$$

$$\begin{aligned}
 &0.01 < r < 0.2 \\
 &|U_{e3}| < 0.2 \\
 &0.24 < \tan^2 \theta_{12} < 0.89 \\
 &0.33 < \tan^2 \theta_{23} < 3.3
 \end{aligned}
 \tag{LA} \tag{6}$$

The boundaries of these windows are close to the 3σ limits on the corresponding observable quantity. The test is successfully passed if $O_i(\mathcal{P})$ are in the above windows, for all $i = 1, \dots, 4$. We will study the dependence on the choice made in eqs. (5,6), by analyzing the distributions of the points generated for each observable. We then estimate V_S/V from the ratio between the number of successful trials over the

total number of attempts. Notice that we do not extend our test to the remaining fermion masses and mixing angles, though the models considered can also reproduce, at the level of order of magnitudes, charged lepton masses, quark masses and mixing angles. With the interval \mathcal{I} fixed at its reference value, $[0.5, 2]$, the different models are compared at their best performance, after optimizing for each model the value of the symmetry breaking parameters λ and λ' .

3.1 LOW solution

In fig. 1 we compare the success rates for the LOW solution. In this figure the anarchical or semi-anarchical models do not appear simply because their rates of success are negligible on the scale of the figure.

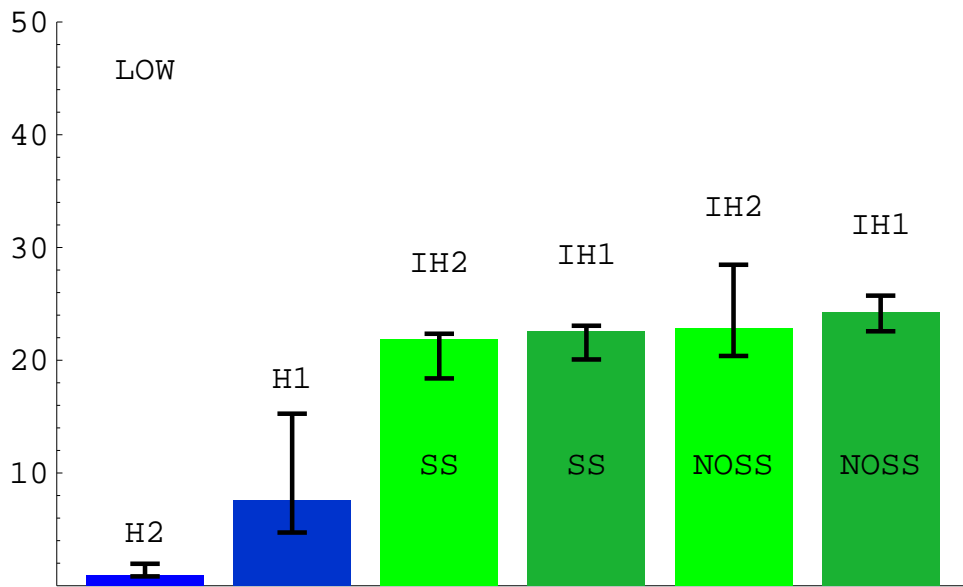


Figure 1: Relative success rates for the LOW solution. The sum of the rates has been normalized to 100. The results correspond to the default choice $\mathcal{I} = [0.5, 2]$, and to the following values of $\lambda = \lambda'$: 0.1, 0.15, 0.03, 0.04, 0.05, 0.06 for the models $H_{(SS,II)}$, $H_{(SS,I)}$, $IH_{(SS,II)}$, $IH_{(SS,I)}$, $IH_{(NOSS,II)}$ and $IH_{(NOSS,I)}$, respectively. The error bars represent the linear sum of the systematic error due to the choice of \mathcal{I} and the statistical error (see text). The results for the A and SA models are below 0.01, independently from \mathcal{I} and from (λ, λ') , and are not displayed.

It is clear that, if the future experimental results will indicate the LOW solution as the preferred one, then anarchical or semi-anarchical schemes will be completely

inadequate to describe the data. It would be natural in that case to adopt a model where the large gap between the atmospheric and the solar oscillation frequencies is built in as a result of a symmetry. What is striking about the results displayed in fig. 1 is the ability of the IH models, both in the SS and in the NOSS versions, to reproduce the data. An appropriate choice for λ (λ') is completely successful in reproducing r . U_{e3} is numerically close to r and easily respects the present bound. Moreover, $\tan^2 \theta_{12}$ is very close to 1, due to the pseudo-Dirac structure of the 12 sector. Only the $\tan^2 \theta_{23}$ distribution shows some flatness and contributes to deplete the success rate. It is worth stressing that $\tan^2 \theta_{12}$ is so strongly peaked around 1, that any significant deviation from $\tan^2 \theta_{12} = 1$ in the data would provide a severe difficulty for the IH schemes. The H model has a smaller success rate (still much larger than that of the A and SA models), but has smoother distributions for the four observables and is less sensitive than IH to variations of the experimental data. The error bars in fig. 1 are dominated by the systematic effects, which have been estimated by varying the interval \mathcal{I} . We considered four possibilities: $\mathcal{I} = [0.5, 2]$ (default), $\mathcal{I} = [0.8, 1.2]$, $\mathcal{I} = [0.95, 1.05]$, and $\mathcal{I} = [0, 1]$. To the highest (lowest) rate of each model we then add (subtract) linearly the statistical error. The latter is usually smaller than the systematic error. Further details are reported in appendix A.

3.2 LA solution

The success rates for the LA solutions are displayed in fig. 2 and 3, separately for the NOSS and SS cases. The two sets of models have been individually normalized to give a total rate 100. Before normalization the total success rates for NOSS and for SS were in the ratio 1.7:1 (see also appendix A). Although the gaps between the rates of different models are reduced compared to the LOW case, nevertheless a clear pattern emerges from these figures. The present data are most easily described by the IH schemes in their NOSS version. Their performances are better by a factor of 10-30 with respect to the last classified, the anarchical models. The ability of the IH schemes in describing the data can be appreciated from the distributions of the four observables, which, for $\text{IH}_{(\text{NOSS,II})}$ and $\lambda = \lambda' = 0.25$, are displayed in fig. 4.

The observables r and U_{e3} are strongly correlated. Actually, as discussed in ref. [1, 20] and shown in table 2, in inversely hierarchical models U_{e3} is typically of order r . Therefore, once λ and λ' have been tuned to fit r , this choice automatically provides a good fit to U_{e3} . Moreover, similarly to the case of the LOW solution, $\tan^2 \theta_{12}$ is peaked around 1. At present $\tan^2 \theta_{12} = 1$ is excluded for the LA solution, but, thanks to the width of the distribution, the experimentally allowed window is sufficiently populated. The width of the distribution is almost entirely dominated

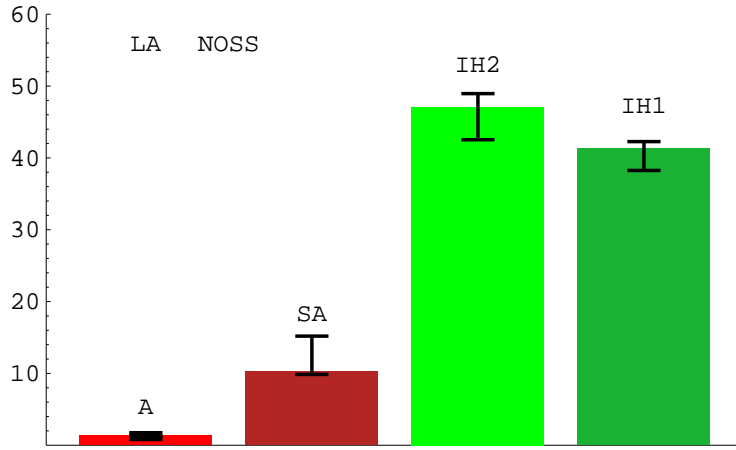


Figure 2: Relative success rates for the LA solution, without see-saw. The sum of the rates has been normalized to 100. The results correspond to the default choice $\mathcal{I} = [0.5, 2]$, and to the following values of $\lambda = \lambda'$: 0.2, 0.2, 0.25, 0.3 for the models A_{NOSS} , SA_{NOSS} , $IH_{(\text{NOSS},\text{II})}$, and $IH_{(\text{NOSS},\text{I})}$, respectively (in our notation there are no $H_{(\text{NOSS},\text{I})}$, $H_{(\text{NOSS},\text{II})}$ models). The error bars represent the linear sum of the systematic error due to the choice of \mathcal{I} and the statistical error (see text).

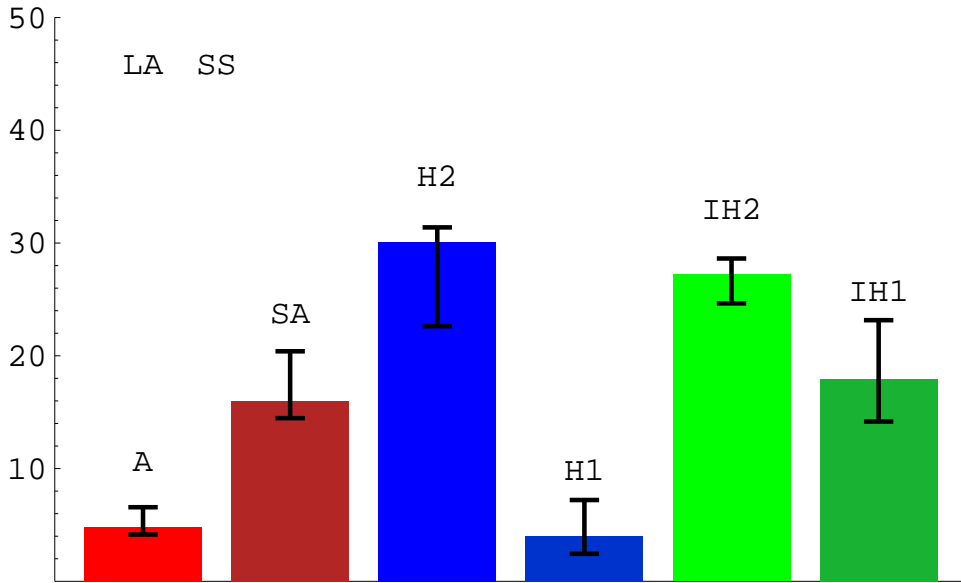


Figure 3: Relative success rates for the LA solution, with see-saw. The sum of the rates has been normalized to 100. The results correspond to the default choice $\mathcal{I} = [0.5, 2]$, and to the following values of $\lambda = \lambda'$: 0.2, 0.3, 0.35, 0.5, 0.15, 0.2 for the models A_{SS} , SA_{SS} , $H_{(\text{SS},\text{II})}$, $H_{(\text{SS},\text{I})}$, $IH_{(\text{SS},\text{II})}$ and $IH_{(\text{SS},\text{I})}$, respectively. The error bars represent the linear sum of the systematic error due to the choice of \mathcal{I} and the statistical error (see text).

$\mathbf{IH}_{(\text{NOSS,II})}$

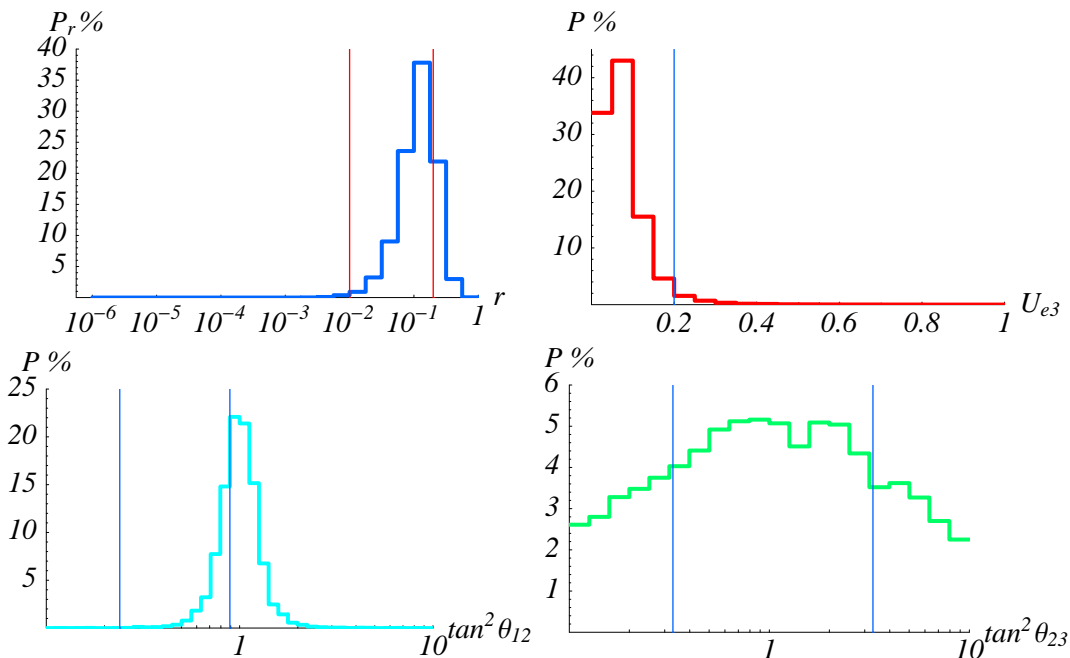


Figure 4: Distributions for $\mathbf{IH}_{(\text{NOSS,II})}$, $\mathcal{I} = [0.5, 2]$, $\lambda = \lambda' = 0.25$, obtained with 10000 points \mathcal{P} .

by the effect coming from the diagonalization of the charged lepton sector. Indeed, by turning off the small parameters λ and λ' in the mass matrix for the charged leptons, we get a vanishing success rate for $\mathbf{IH}_{(\text{NOSS,I})}$, whereas the rate for $\mathbf{IH}_{(\text{NOSS,II})}$ decreases by more than one order of magnitude. It is worth stressing that even a moderate further departure of the window away from $\tan^2 \theta_{12} = 1$ could drastically reduce the success rates of the IH schemes. Finally, the $\tan^2 \theta_{23}$ distribution is rather flat, with a moderate peak in the currently favoured interval. All the IH models, with or without see-saw, have distributions similar to those shown in fig. 4. In particular the $\tan^2 \theta_{23}$ distribution of fig. 4 is qualitatively common to all U(1) models. This reflects the fact that the large angle θ_{23} is induced by the equal charges $F(\bar{5}_2) = F(\bar{5}_3)$, a feature shared by all the models we have considered. To appreciate the relevant correlations, the distributions for the model $\mathbf{IH}_{(\text{NOSS,II})}$ are also displayed in fig. 5, as scatter plots in the planes (U_{e3}, r) , $(\tan^2 \theta_{12}, r)$ and $(\tan^2 \theta_{23}, r)$.

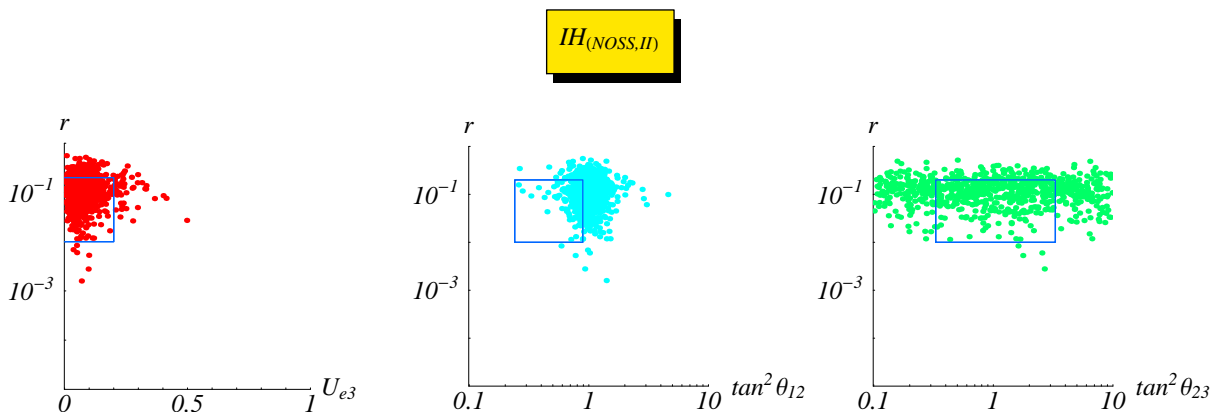


Figure 5: Scatter plots in the planes (U_{e3}, r) , $(\tan^2 \theta_{12}, r)$ and $(\tan^2 \theta_{23}, r)$ for $\text{IH}_{(\text{NOSS,II})}$, $\mathcal{I} = [0.5, 2]$, $\lambda = \lambda' = 0.25$, obtained with 1000 points \mathcal{P} . The box shows the experimental window for LA.

Without see-saw mechanism, the next successful model is the semi-anarchical model SA, whose distributions are displayed in fig. 6 (in our notation there are no $\text{H}_{\text{NOSS,I(II)}}$ models). Compared to the IH case, the $\tan^2 \theta_{12}$ distribution has no pronounced peak. Possible shifts in the central value of $\tan^2 \theta_{12}$ would not drastically modify the results for the SA model. The U_{e3} distribution is peaked around $\lambda = 0.2$ with tails that exceed the present experimental bound. The r distribution is centered near $r = 1$. Finally, the anarchical scheme in its NOSS version is particularly disfavoured, due to its tendency to predict r close to 1 and also due to U_{e3} , that presents a broad distribution with a preferred value of about 0.5.

The overall picture changes significantly if the LA solution is realized in the context of the see-saw mechanism, as illustrated in fig. 3. The IH models are still rather successful. Compared to the NOSS case, the IH_{SS} models slightly prefer higher values of r and, due to a smaller $\lambda = \lambda'$, they have very narrow $\tan^2 \theta_{12}$ distributions. This can be seen from the scatter plots of fig. 7. The other distributions are similar to those of figs. 4 and 5. We observe that while most of the points in fig. 7 are centered around $U_{e3} \approx O(\lambda^2)$, there is also a small region clustered at $U_{e3} \approx 0.6$.

Equally good or even better results are obtained by the $\text{H}_{(\text{SS,I})}$ model, with distributions shown in fig. 8 and 9. We see that, at variance with the IH models, $\tan^2 \theta_{12}$ is not spiky, which results in a better stability of the model against variation of the experimental results. The preferred value of r is close to the lower end of the experimental window. The U_{e3} distribution is nicely peaked around λ^2 .

SA_{NOSS}

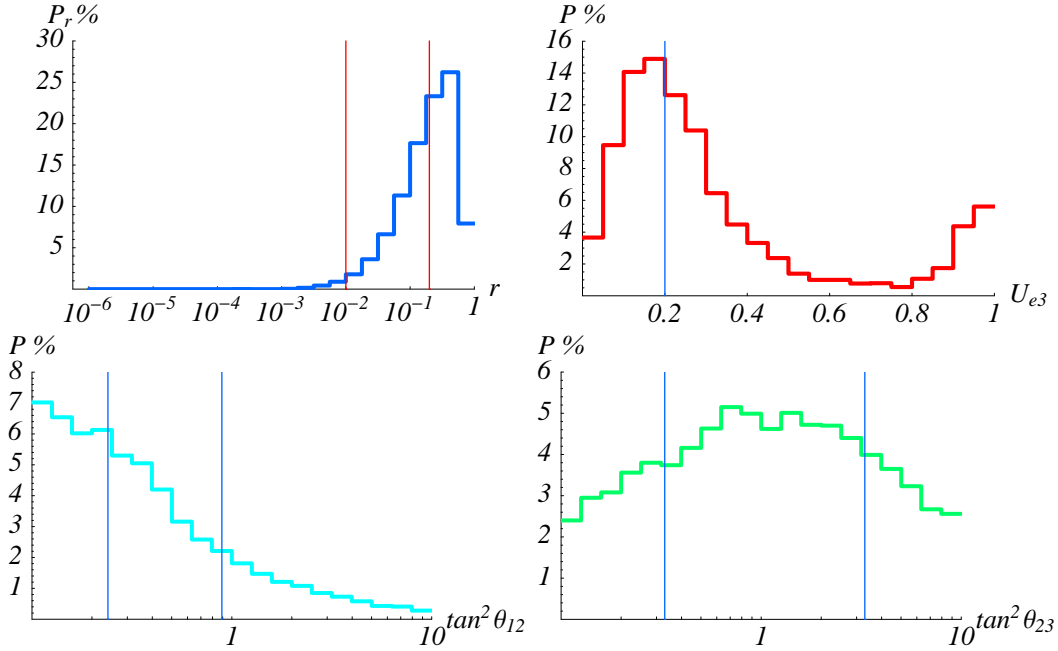


Figure 6: Distributions for the semi-anarchical no-see-saw SA_{NOSS}, $\mathcal{I} = [0.5, 2]$, $\lambda = \lambda' = 0.2$, obtained with 10000 points \mathcal{P} .

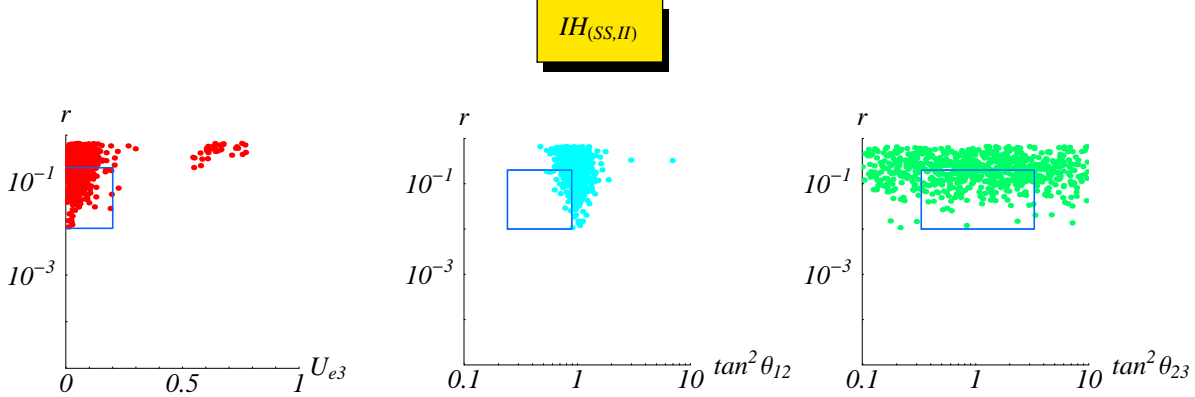


Figure 7: Scatter plots in the planes (U_{e3}, r) , $(\tan^2 \theta_{12}, r)$ and $(\tan^2 \theta_{23}, r)$ for $IH_{(SS,II)}$, $\mathcal{I} = [0.5, 2]$, $\lambda = \lambda' = 0.15$, obtained with 1000 points \mathcal{P} . The box shows the experimental window for LA.

The SA_{SS} model is significantly outdistanced from $H_{(SS,II)}$, $IH_{(SS,II)}$ and $IH_{(SS,I)}$. It is particularly penalized by the U_{e3} distribution, centered around $\lambda = 0.3$. Finally, the least favoured models are $H_{(SS,I)}$ and A_{SS} . The model $H_{(SS,I)}$ fails both in U_{e3}

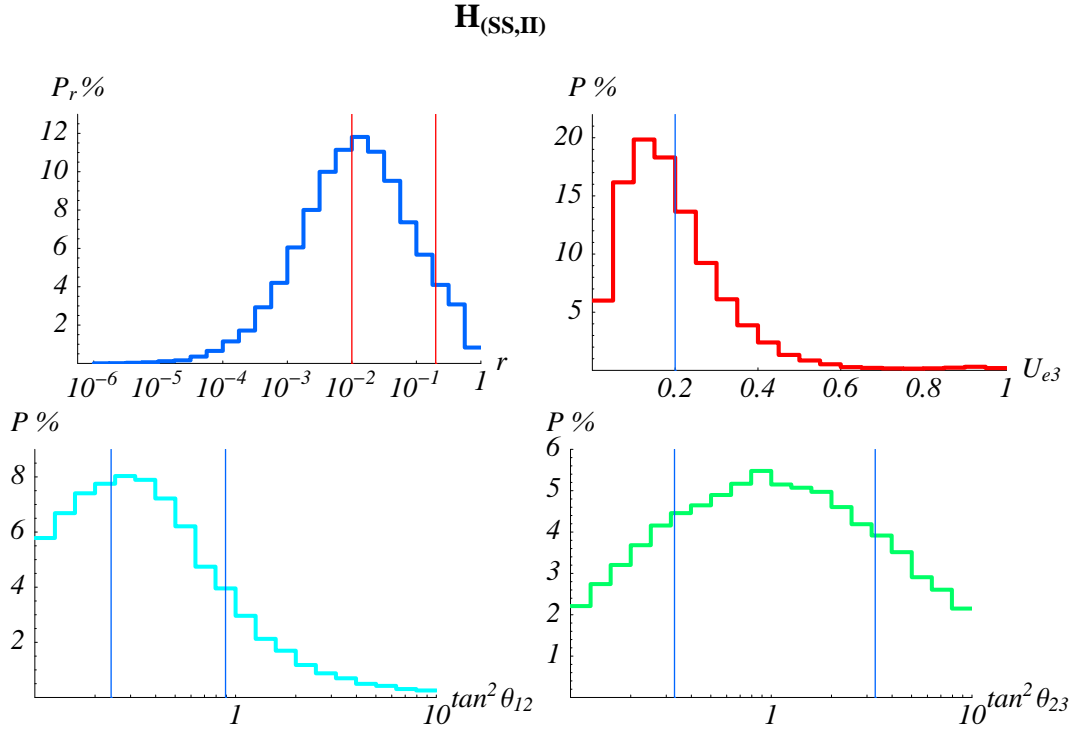


Figure 8: Distributions for $H_{(SS,II)}$, $\mathcal{I} = [0.5, 2]$, $\lambda = \lambda' = 0.35$, obtained with 50000 points \mathcal{P} .

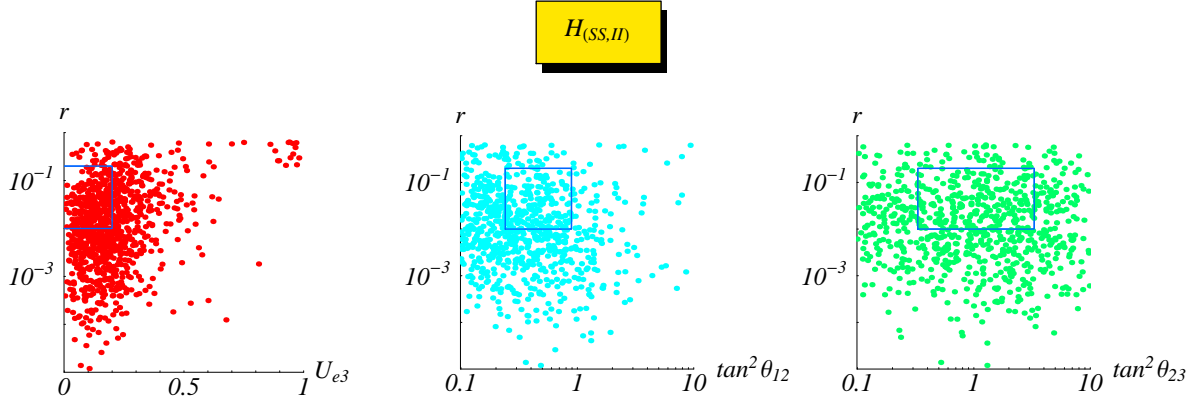


Figure 9: Scatter plots in the planes (U_{e3}, r) , $(\tan^2 \theta_{12}, r)$ and $(\tan^2 \theta_{23}, r)$ for $H_{(SS,II)}$, $\mathcal{I} = [0.5, 2]$, $\lambda = \lambda' = 0.35$, obtained with 1000 points \mathcal{P} . The box shows the experimental window for LA.

(see fig. 10), which tends to be too large for the preferred value of $\lambda = \lambda' = 0.5$ and in $\tan^2 \theta_{12}$. The A_{SS} model, as its NOSS version, suffers especially from the U_{e3} distribution (see fig. 10) which is roughly centered at 0.5, with only few percent

of the attempts falling within the present experimental bound. A large U_{e3} can be regarded as a specific prediction of anarchy and any possible improvement of the bound on $|U_{e3}|$ will wear away the already limited success rate of the model. The distributions in $\tan^2 \theta_{12}$ and $\tan^2 \theta_{23}$ are equally broad and peaked around 1. Compared to the NOSS case, A_{SS} has a better r distribution, well located inside the allowed window.

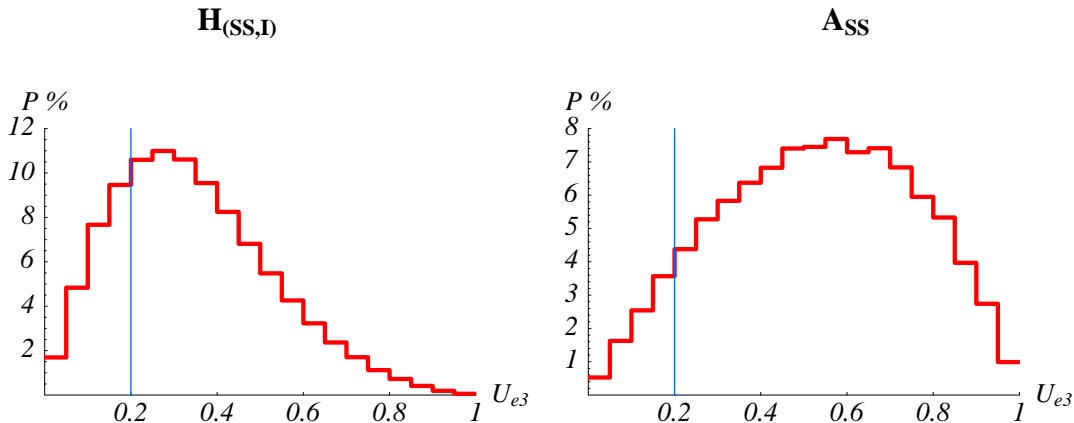


Figure 10: U_{e3} Distributions for $H_{(SS,I)}$ ($\lambda = \lambda' = 0.5$) and A_{SS} ($\lambda = \lambda' = 0.2$), $\mathcal{I} = [0.5, 2]$, obtained with 50000 points \mathcal{P} .

As another criterion for evaluating the quality of a model, we address the issue of the stability of the observables O_i with respect to small fluctuations of the set of coefficients \mathcal{P} . Notice that the random coefficients to be put in front of the powers of λ, λ' stand for the combined result of a fundamental theory of flavour, present at a certain scale Λ , and of an evolution from Λ down to m_Z . It would thus be natural if the physical observables O_i were stable under small perturbations of the coefficients, $\Delta\mathcal{P}$, around a given successful representative set \mathcal{P}_0 .

This is illustrated for the seesaw case in fig. 11, where we compare the models $IH_{(SS,I)}$, $H_{(SS,I)}$ and A_{SS} . The blue dot refers to the observables O_i which follow from a typical successful configuration for LA, \mathcal{P}_0 . The 40 points in red, light blue and green are the result of adding to \mathcal{P}_0 random perturbations $\Delta\mathcal{P}$ with $|\Delta\mathcal{P}| = |\mathcal{P}|/10$ and random phases. The yellow dots correspond to $|\Delta\mathcal{P}| = |\mathcal{P}|/2$. As appears from the scatter plots, $IH_{(SS,I)}$ is very stable: as already argued in the above discussion, actually it is even dangerously stable with respect to the prediction for $\tan^2 \theta_{12}$. If models with hierarchy display a sufficient degree of stability, anarchical ones are much less stable, in particular with respect to the predictions for U_{e3} and $\tan^2 \theta_{12}$.

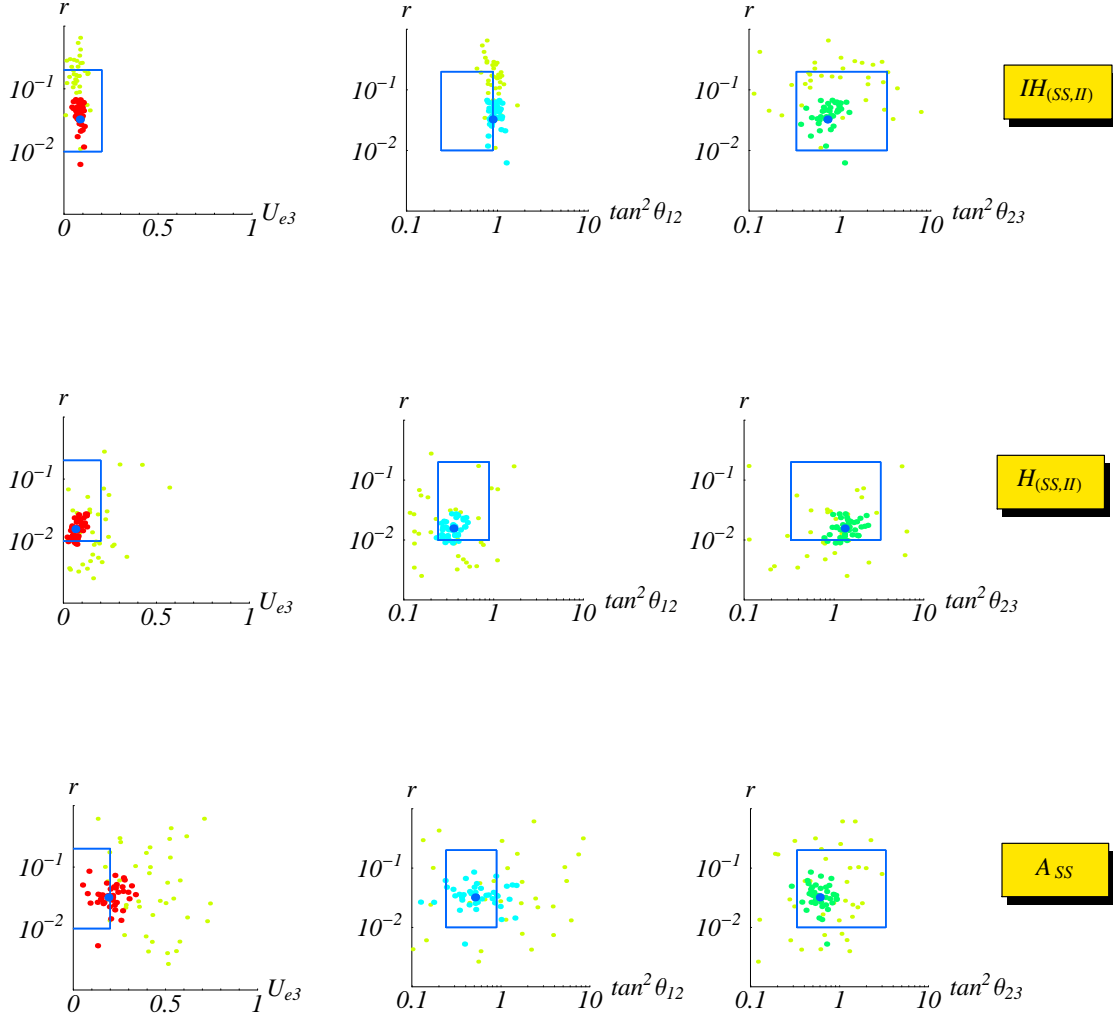


Figure 11: Results of the stability test in the planes (U_{e3}, r) , $(\tan^2 \theta_{12}, r)$ and $(\tan^2 \theta_{23}, r)$ for $\text{IH}_{(SS,II)}$ ($\lambda = \lambda' = 0.15$), $H_{(SS,II)}$ ($\lambda = \lambda' = 0.35$) and A_{SS} ($\lambda = \lambda' = 0.2$), $\mathcal{I} = [0.5, 2]$ (see text).

As shown in fig. 12, the non see-saw case enhances these features: $\text{IH}_{(\text{NOSS},II)}$ is extremely stable, while A_{NOSS} is highly unstable. For the latter, in particular, even with the small fluctuation considered in the figures, $\tan^2 \theta_{12}$ spans from .1 to 10. Thus, the criterion of stability supports the same ratings of models previously obtained by only considering total rates and distributions.

As a general comment we observe that our results are rather stable with respect to the choice of the interval \mathcal{I} . With only one exception, namely the crossing between $H_{(SS,I)}$ and A_{SS} , the relative position of the different models, according to their ability in describing the data, does not vary when we shrink \mathcal{I} , or when we extend

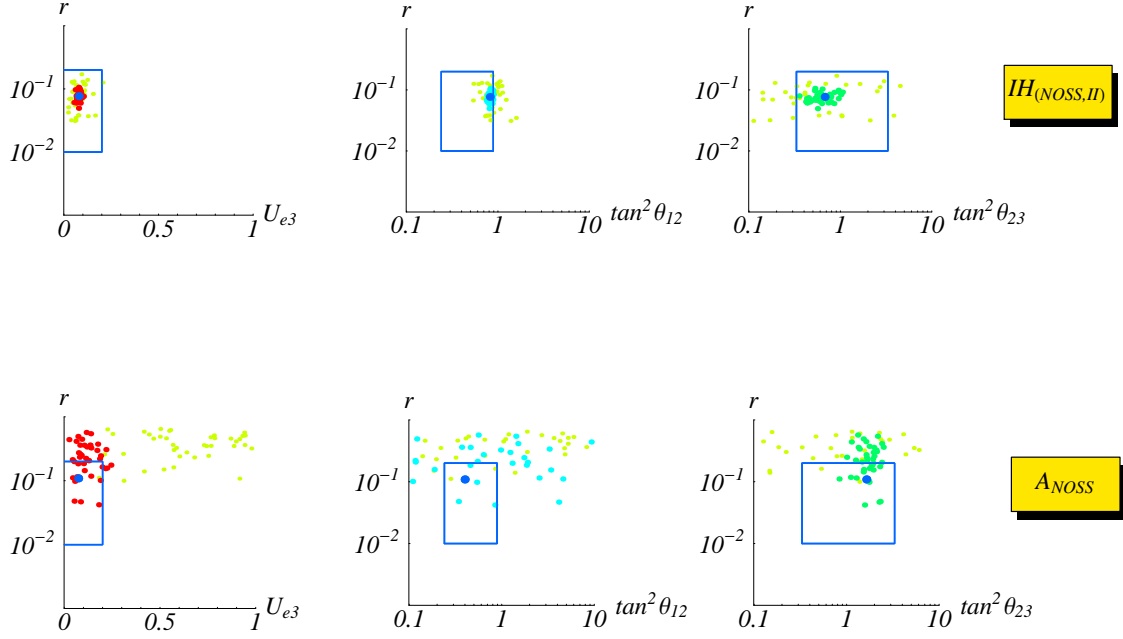


Figure 12: Results of the stability test in the planes (U_{e3}, r) , $(\tan^2 \theta_{12}, r)$ and $(\tan^2 \theta_{23}, r)$ for $IH_{(NOSS,II)}$ ($\lambda = \lambda' = 0.25$) and A_{NOSS} ($\lambda = \lambda' = 0.2$), $\mathcal{I} = [0.5, 2]$ (see text).

it to cover the full circle of radius 1³. This stability would be partially upset by restricting to the case of real coefficients \mathcal{P} . In that case the relative rates are comparable to those obtained in the complex case only for sufficiently wide intervals \mathcal{I} , typically $\mathcal{I} \approx [-1/\sqrt{\lambda}, -\sqrt{\lambda}] \cup [\sqrt{\lambda}, 1/\sqrt{\lambda}]$. If we further squeeze \mathcal{I} around ± 1 the rates of all models tend to zero. In the real case, the distribution of $\tan^2 \theta_{23}$ is very sensitive to the width of the extraction interval \mathcal{I} . Indeed, in the flavour symmetry basis, charged leptons and light neutrinos mass matrices are both diagonalised by a 23 mixing angle which tends to $\pi/4$ when \mathcal{I} is squeezed to 1. As an effect, in this limit the distribution of θ_{23} is almost empty around $\pi/4$ and presents two peaks at 0 and $\pi/2$. On the contrary, in the complex case the distribution of θ_{23} is quite insensitive to the width of \mathcal{I} thanks to the smearing effect of the phases.

³The results for $\mathcal{I} = [0, n]$ are independent on n , since changing n amounts to perform a renormalization of all mass matrices by a common overall scale, which is not felt by the observables we have used in our analysis.

4 Conclusion

If a large gap between the solar and atmospheric frequencies for neutrino oscillations were finally to be established by experiment then this fact would immediately suggest that neutrino masses are hierarchical, similar to quark and charged lepton masses. In fact very small mass squared differences among nearly degenerate neutrino states are difficult to obtain and make stable under running in the absence of an ad hoc symmetry. Moreover, the presence of very small mixing angles would also indicate a hierarchical pattern. At present, the SA solution of solar neutrino oscillations is disfavoured so that 2 out of 3 mixing angles appear to be large and only one appears to be small, although the present limit is not terribly constraining. However, in the case of the LA solution for solar neutrino oscillations, the ratio r of the solar to atmospheric frequencies is not so small and it has been suggested that possibly this solution does not require a symmetry to be generated. In the anarchical framework the smallness of U_{e3} , assumed not too pronounced, and that of r , are considered as accidental (the see-saw mechanism helps in this respect because the product of 3 matrices sizeably broadens the r distribution). In the present study we have examined in quantitative terms the relative merits of anarchy and of different implementations of hierarchy in reproducing the observed features of the LA solution. For our analysis we have adopted the framework of $SU(5) \times U(1)_F$ which is flexible enough, by suitable choices of the flavour charges, to reproduce all interesting types of hierarchy and also of anarchy. This framework allows a statistical comparison of the different schemes under, as far as possible, homogeneous conditions. The rating of models in terms of their statistical rates of success is clearly a questionable procedure. After all Nature does not proceed at random and a particular mass pattern that looks odd could arise due to some deep dynamical reason. However, the basis for anarchy as a possible description of the LA solution can only be formulated in statistical terms. Therefore it is interesting to compare anarchy versus hierarchy on the same grounds. We have considered models both with normal and with inverse hierarchies, with and without see-saw, with one or two flavons, and compared them with the case of anarchy and of semi-anarchy (models where there is no structure in 2-3 but only in 2-3 vs 1). The stability of our results has been tested by considering different options for the statistical procedure and also by studying the effect on each type of model of small parameter changes.

Our conclusion is that, for the LA solution, the range of r and the small upper limit on U_{e3} are sufficiently constraining to make anarchy neatly disfavoured with respect to models with built-in hierarchy. If only neutrinos are considered, one might counterargue that hierarchical models have at least one more parameter than anarchy, in our case the parameter λ . However, if one looks at quarks and leptons together, as in the GUT models that we consider, then the same parameter that

plays the role of an order parameter for the CKM matrix, for example, the Cabibbo angle, can be successfully used to reproduce also the LA hierarchy. On the one hand, it is interesting that the amount of hierarchy needed for the LA solution is just a small power of the Cabibbo angle. On the other hand, if all fermion masses and mixings are to be reproduced, a similar parameter is also needed in anarchical models, where all the quark and lepton mass structure arises from the charges of Ψ_i^{10} . In comparison to anarchy even the limited amount of structure present in semi-anarchical models already improves the performance a lot. And the advantage is further increased when more structure is added as in inverse hierarchy models, or models with normal hierarchy and automatic suppression of the 23 determinant. In the see-saw case all these types of hierarchical models have comparable rates of success (except for $H_{(SS,I)}$). In the non-see-saw versions of inverse hierarchy the performance is even better. An experimental criterion that could eventually decide between normal and inverse hierarchy models is the closeness of the solar angle θ_{12} to its maximal value. If the data moves away from $\pi/4$ the probability of inverse hierarchy will rapidly drop in comparison to hierarchical models.

Acknowledgments

We would like to thank Francesco Vissani for useful discussions and for participating in the early stages of the present work. F.F. and I.M. thank the CERN TH division for its hospitality during july and august 2002, when this project was developed. This work is partially supported by the European Programs HPRN-CT-2000-00148 and HPRN-CT-2000-00149.

Appendix: raw data

In this section we list the results of our numerical analysis, for the case of complex random coefficients \mathcal{P} . In particular we detail the dependence of the success rates on the size of the window \mathcal{I} that specifies the absolute value of the coefficients \mathcal{P} . In most cases the ‘systematic’ error due to the choice of \mathcal{I} is larger than the statistical error. The latter is given by $\delta P/P = 1/\sqrt{N_s}$, where $P = 100 \cdot N_s/N$ is the success rate and N_s is the number of successes in N trials. We chose $N = 10000, 30000, 50000$ respectively, for the LOW solution, for LA without see-saw and for LA with see-saw. When fitting the LOW solution, the results for the anarchical and semi-anarchical models do not depend on λ or λ' .

Table 3: Success rates for the LOW solution, with the see-saw mechanism.

		success rate			
model	$\lambda(= \lambda')$	$\mathcal{I} = [0.5, 2]$	$\mathcal{I} = [0.8, 1.2]$	$\mathcal{I} = [0.95, 1.05]$	$\mathcal{I} = [0, 1]$
A_{SS}	-	< 0.01	< 0.01	< 0.01	< 0.01
SA_{SS}	-	< 0.01	< 0.01	< 0.01	< 0.01
$H_{(SS,II)}$	0.1	1.7 ± 0.1	2.8 ± 0.2	2.8 ± 0.2	1.6 ± 0.1
$H_{(SS,I)}$	0.15	14.4 ± 0.4	21.6 ± 0.5	23.0 ± 0.5	7.6 ± 0.3
$IH_{(SS,II)}$	0.03	41.6 ± 0.6	30.3 ± 0.6	29.0 ± 0.5	31.2 ± 0.6
$IH_{(SS,I)}$	0.04	42.9 ± 0.7	32.8 ± 0.6	31.6 ± 0.6	32.0 ± 0.6

Table 4: Success rates for the LOW solution, without the see-saw mechanism.

		success rate			
A_{NOSS}	-	< 0.01	< 0.01	< 0.01	< 0.01
SA_{NOSS}	-	< 0.01	< 0.01	< 0.01	< 0.01
$IH_{(NOSS,II)}$	0.05	43.4 ± 0.7	33.3 ± 0.6	32.1 ± 0.6	42.9 ± 0.7
$IH_{(NOSS,I)}$	0.06	46.1 ± 0.7	36.5 ± 0.6	35.5 ± 0.6	38.8 ± 0.6

Table 5: Success rates for the LA solution, without see-saw mechanism.

		success rate			
A_{NOSS}	0.2	0.33 ± 0.03	0.23 ± 0.03	0.25 ± 0.03	0.26 ± 0.03
SA_{NOSS}	0.2	2.5 ± 0.1	2.9 ± 0.1	2.6 ± 0.1	2.5 ± 0.1
$IH_{(NOSS,II)}$	0.25	11.4 ± 0.2	8.8 ± 0.2	8.2 ± 0.2	10.2 ± 0.2
$IH_{(NOSS,I)}$	0.3	10.0 ± 0.2	7.9 ± 0.2	7.7 ± 0.2	8.4 ± 0.2

Table 6: Success rates for the LA solution, with see-saw mechanism.

		success rate			
model	$\lambda(=\lambda')$	$\mathcal{I} = [0.5, 2]$	$\mathcal{I} = [0.8, 1.2]$	$\mathcal{I} = [0.95, 1.05]$	$\mathcal{I} = [0, 1]$
A_{SS}	0.2	0.69 ± 0.04	0.62 ± 0.04	0.63 ± 0.04	0.63 ± 0.04
SA_{SS}	0.3	2.30 ± 0.07	2.12 ± 0.07	2.07 ± 0.06	1.99 ± 0.06
$H_{(SS,II)}$	0.35	4.33 ± 0.09	4.35 ± 0.09	4.34 ± 0.09	2.36 ± 0.07
$H_{(SS,I)}$	0.5	0.58 ± 0.03	0.88 ± 0.04	0.97 ± 0.04	0.27 ± 0.02
$IH_{(SS,II)}$	0.15	3.92 ± 0.09	3.97 ± 0.09	4.06 ± 0.09	2.57 ± 0.07
$IH_{(SS,I)}$	0.2	2.58 ± 0.07	2.24 ± 0.07	2.07 ± 0.06	2.26 ± 0.07

References

- [1] For a review, see: G. Altarelli and F. Feruglio, arXiv:hep-ph/0206077.
- [2] A. Strumia, C. Cattadori, N. Ferrari and F. Vissani, *Phys. Lett. B* **541** (2002) 327 [arXiv:hep-ph/0205261].
- [3] S. A. Dazeley [KamLAND Collaboration], arXiv:hep-ex/0205041.
- [4] The LSND collaboration, hep-ex/0104049.
- [5] The Karmen collaboration, *Nucl. Phys. Proc. Suppl.* **91**, 191 (2000).
- [6] P. Spentzouris, *Nucl. Phys. Proc. Suppl.* **100**, 163 (2001).
- [7] C. H. Albright and S. M. Barr, *Phys. Rev. D* **58**, 013002 (1998); C. H. Albright, K. S. Babu and S. M. Barr, *Phys. Rev. Lett.* **81**, 1167 (1998); N. Irges, S. Lavignac and P. Ramond, *Phys. Rev. D* **58**, 035003 (1998); G. Altarelli and F. Feruglio, *Phys. Lett. B* **439**, 112 (1998) and *JHEP* **9811**, 021 (1998); P. H. Frampton and A. Rasin, *Phys. Lett. B* **478**, 424 (2000).
- [8] A.Y. Smirnov, *Phys. Rev. D* **48** (1993) 3264; S. F. King, *Phys. Lett. B* **439** (1998) 350; S. Davidson and S. F. King, *Phys. Lett. B* **445** (1998) 191; Q. Shafi and Z. Tavartkiladze, *Phys. Lett. B* **451** (1999) 129; G. Altarelli, F. Feruglio and I. Masina, *Phys. Lett. B* **472**, 382 (2000); S. F. King, *Nucl. Phys. B* **562**, 57 (1999); *Nucl. Phys. B* **576**, 85 (2000); hep-ph/0204360;
- [9] The HEIDELBERG–MOSCOW collaboration, H.V. Klapdor-Kleingrothaus *et al.* *Eur. Phys. J.*, **A12**, 147 (2001); C. E. Aalseth *et al.* [16EX Collaboration], hep-ex/0202026; H.V. Klapdor-Kleingrothaus *et al.*, *Mod. Phys. Lett.*, **A37** 2409 (2001). See also: C. E. Aalseth *et al.*, hep-ex/0202018 and appendix of F. Feruglio, A. Strumia and F. Vissani, *Nucl. Phys. B* **637** (2002) 345 [arXiv:hep-ph/0201291].
- [10] F. Vissani, hep-ph/9708483; H. Georgi and S. L. Glashow, *Phys. Rev. D* **61**, 097301 (2000);
- [11] L. J. Hall, H. Murayama and N. Weiner, *Phys. Rev. Lett.* **84** (2000) 2572 [arXiv:hep-ph/9911341].
- [12] The CHOOZ collaboration *Phys. Lett. B* **466**, 415 (1999); see also: The PALO VERDE collaboration *Phys. Rev. Lett.* , **84**, 3764 (2000).
- [13] C. D. Froggatt and H. B. Nielsen, *Nucl. Phys. B* **147**, 277 (1979).

- [14] J. Sato and T. Yanagida, *Phys. Lett. B* **430**, 127 (1998); J. K. Elwood, N. Irges and P. Ramond, *Phys. Rev. Lett.* **81**, 5064 (1998); Z. Berezhiani and A. Rossi, *JHEP* **9903**, 002 (1999); G. Altarelli and F. Feruglio, *Phys. Lett. B* **451**, 388 (1999); M. Bando and T. Kugo, *Prog. Theor. Phys.* **101**, 1313 (1999); G. Altarelli, F. Feruglio and I. Masina, *JHEP* **0011**, 040 (2000); I. Masina, *Int. J. Mod. Phys. A* **16** (2001) 5101 [arXiv:hep-ph/0107220].
- [15] See also: J. Bijnens and C. Wetterich, *Nucl. Phys.* B147, 292 (1987); M. Leurer, Y. Nir and N. Seiberg, *Nucl. Phys. B* **398**, 319 (1993); *Nucl. Phys. B* **420**, 468 (1994); L. E. Ibanez and G. G. Ross, *Phys. Lett. B* **332**, 100 (1994); P. Binetruy and P. Ramond, *Phys. Lett. B* **350**, 49 (1995); E. Dudas, S. Pokorski and C. A. Savoy, *Phys. Lett. B* **356**, 45 (1995); K. Hagiwara and N. Okamura, *Nucl. Phys. B* **548**, 60 (1999); G. K. Leontaris and J. Rizos, *Nucl. Phys. B* **567** (2000) 32; J. M. Mira, E. Nardi and D. A. Restrepo, *Phys. Rev. D* **62**, 016002 (2000). P. Binetruy, S. Lavignac and P. Ramond, *Nucl. Phys. B* **477**, 353 (1996); P. Binetruy, S. Lavignac, S. T. Petcov and P. Ramond, *Nucl. Phys. B* **496**, 3 (1997); Z. Berezhiani and Z. Tavartkiladze, *Phys. Lett. B* **396**, 150 (1997); M. Jezabek and Y. Sumino, *Phys. Lett. B* **440**, 327 (1998); Y. Grossman, Y. Nir and Y. Shadmi, *JHEP* **9810**, 007 (1998); W. Buchmuller and T. Yanagida, *Phys. Lett. B* **445**, 399 (1999); C. D. Froggatt, M. Gibson and H. B. Nielsen, *Phys. Lett. B* **446**, 256 (1999); K. Choi, K. Hwang and E. J. Chun, *Phys. Rev. D* **60**, 031301 (1999); S. Lola and G. G. Ross, *Nucl. Phys. B* **553**, 81 (1999); Y. Nir and Y. Shadmi, *JHEP* **9905**, 023 (1999); B. Stech, *Phys. Rev. D* **62**, 093019 (2000); S. F. King and M. Oliveira, *Phys. Rev. D* **63**, 095004 (2001); M. Tanimoto, *Phys. Lett. B* **501**, 231 (2001); M. Bando and N. Maekawa, *Prog. Theor. Phys.* **106**, 1255 (2001). H. B. Nielsen and Y. Takanishi, *Phys. Scripta* **T93**, 44 (2001); W. Grimus and L. Lavoura, *JHEP* **0107**, 045 (2001) and hep-ph/0204070.
- [16] For related works, see: N. Haba and H. Murayama, *Phys. Rev. D* **63** (2001) 053010 [arXiv:hep-ph/0009174]. M. Hirsch, arXiv:hep-ph/0102102. M. Hirsch and S. F. King, *Phys. Lett. B* **516** (2001) 103 [arXiv:hep-ph/0102103]. F. Visani, *Phys. Lett. B* **508** (2001) 79 [arXiv:hep-ph/0102236]. R. Rosenfeld and J. L. Rosner, *Phys. Lett. B* **516** (2001) 408 [arXiv:hep-ph/0106335]. F. Visani, arXiv:hep-ph/0111373. V. Antonelli, F. Caravaglios, R. Ferrari and M. Picariello, arXiv:hep-ph/0207347.
- [17] R. Barbieri, L. J. Hall, D. R. Smith, A. Strumia and N. Weiner, *JHEP* **9812**, 017 (1998); R. Barbieri, L. J. Hall and A. Strumia, *Phys. Lett. B* **445**, 407 (1999); See also: Ya. B. Zeldovich, *Dok. Akad. Nauk. CCCP* 86, 505 (1952); E.J. Konopinsky, H. Mahmoud *Phys. Rev.* 92, 1045 (1953); A. Zee, *Phys. Lett.* B93,

- 389 (1980); S. Petcov, *Phys. Lett.* B100, 245 (1982); A. S. Joshipura and S. D. Rindani, *Eur. Phys. J. C* **14**, 85 (2000); R. N. Mohapatra, A. Perez-Lorenzana and C. A. de Sousa Pires, *Phys. Lett. B* **474**, 355 (2000); Q. Shafi and Z. Tavartkiladze, *Phys. Lett. B* **482**, 145 (2000); hep-ph/0101350; A. Ghosal, *Phys. Rev. D* **62**, 092001 (2000); L. Lavoura, *Phys. Rev. D* **62**, 093011 (2000); L. Lavoura and W. Grimus, *JHEP* **0009**, 007 (2000) and *Phys. Rev. D* **62**, 093012 (2000); S. F. King and N. N. Singh, *Nucl. Phys. B* **596**, 81 (2001); J. F. Oliver and A. Santamaria, *Phys. Rev. D* **65**, 033003 (2002); K. S. Babu and R. N. Mohapatra, hep-ph/0201176.
- [18] T. Yanagida, in *Proc. of the Workshop on Unified Theory and Baryon Number in the Universe*, KEK, March 1979; M. Gell-Mann, P. Ramond and R. Slansky, in *Supergravity*, Stony Brook, Sept 1979.
- [19] G. L. Fogli, E. Lisi, D. Montanino and A. Palazzo, *Phys. Rev. D* **64**, 093007 (2001); J. N. Bahcall, M. C. Gonzalez-Garcia and C. Pena-Garay, *JHEP* **0108**, 014 (2001); hep-ph/0111150; V. Barger, D. Marfatia, K. Whisnant and B. P. Wood, hep-ph/0204253; A. Bandyopadhyay, S. Choubey, S. Goswami and D. P. Roy, hep-ph/0204286; J. N. Bahcall, M. C. Gonzalez-Garcia and C. Pena-Garay, hep-ph/0204314; P. Aliani, V. Antonelli, R. Ferrari, M. Picariello and E. Torrente-Lujan, hep-ph/0205053; G. L. Fogli, E. Lisi and A. Marrone, *Phys. Rev. D* **64**, 093005 (2001); M. C. Gonzalez-Garcia, M. Maltoni and C. Pena-Garay, hep-ph/0108073. M. C. Gonzalez-Garcia and Y. Nir, hep-ph/0202058; G. Fogli and E. Lisi in “Neutrino Mass”, Springer Tracts in Modern Physics, ed. by G. Altarelli and K. Winter; G. L. Fogli, G. Lettera, E. Lisi, A. Marrone, A. Palazzo and A. Rotunno, arXiv:hep-ph/0208026.
- [20] S. Lavignac, I. Masina and C. A. Savoy, *Nucl. Phys. B* **633** (2002) 139 [arXiv:hep-ph/0202086].